Spin waves in spin-polarized H↓

J. H. Freed (*)

Laboratoire de Spectroscopie Hertzienne de l'Ecole Normale Supérieure.
24, rue Lhomond, 75230 Paris Cedex, France

Résumé. — Nous présentons une brève revue de résultats, publiés ou non, obtenus à l'Université de Cornell et concernant l'observation d'ondes de spin nucléaire amorties dans un gaz d'hydrogène atomique dont le spin est polarisé.

Abstract. — This is a short review of previous published and unpublished results of our Cornell University group pertaining to the observations of damped nuclear spin-wave modes in spin-polarized atomic hydrogen gas.

The recent observation of nuclear spin-waves in spin polarized H↓ gas by our group at Cornell University [1, 2, 3] may be said to have been indirectly influenced by the pioneering work of Kastler and Brossel on optical pumping. It is, of course true, that the required nuclear spin-polarization of H↓ is achieved by a « chemical pumping » as discussed below, but it is also true that our group drew inspiration from the pioneering work of Laloë, Lhuillier, and Leduc who, motivated by their experimental efforts on spin polarizing ^{3}He gas at low temperatures by optical pumping [4], carried out their fundamental theoretical work on quantum effects in dilute spin-polarized gases at low temperatures [5]. Similar predictions were also made by E. P. Bashkin [6]. These results are described in this volume by Lhuillier and Leduc [7a].

The fascinating properties of H↓ gas are discussed elsewhere in this volume by D. Kleppner [7b] and in recent reviews [8, 9], so we only briefly summarize those properties which are important for the nuclear spin-wave phenomenon. Spin-polarized H↓ is a gas of *atomic* hydrogen in which the electron spins have been aligned by cooling the H atoms to $T \leqslant 0.5$ K in a strong magnetic field, $H_0 \simeq 8$-10 T. The Boltzmann factor guarantees that virtually all the electron spins are « down ». By the Pauli Exclusion Principle, pairwise collisions of H↓ atoms are predominantly repulsive (despite a weak long-range Van der Waals attraction). This repulsion of triplet-spin ($S = 1$) pairs of H atoms prevents their recombination (but see below) and also prevents liquefaction. Thus H↓ is a gas, in fact a nearly ideal gas at the densities studied for which $PV = nRT$! Also, H↓ is a gas of Bosons. Why the composite H↓ atoms behave as Bosons has been outlined simply elsewhere [10], but the spin-wave observations discussed below do confirm this fact experimentally. For such a weakly interacting quantum gas, one might expect to observe a Bose-Einstein Condensation (BEC) if densities are sufficiently high and temperatures are sufficiently low. In particular, one expects BEC when the thermal de Broglie wavelength of H↓ atoms : $\lambda_T = h(2\pi mkT)^{-1/2} \simeq$ the interatomic spacing $\simeq n^{-1/3}$. This leads to $T_c \simeq 1.6 \times 10^{-14}\, n_c^{2/3}$ (e.g. for $n_c \simeq 10^{19}$ cm^{-3}, $T_c \simeq 74$ mK). It has not yet been possible to

(*) Guggenheim Fellow 1984-85, on leave from Cornell University, Ithaca, New York 14853, U.S.A.

achieve densities sufficient for BEC for reasons discussed by Kleppner [7b]. However, a main point of the work of Laloë and co-workers is that even the dilute spin-polarized gas can show significant quantum effects provided only $\lambda \gtrsim d$, where d is a measure of the range of interaction between a colliding pair of atoms, i.e. of the order of atomic sizes. This places no restrictions on the density, but only on the temperature, and the latter can easily be satisfied in the laboratory.

The remaining prerequisite for the observation of nuclear spin-waves is to have the nuclear spins polarized. For fields of *ca.* 10 T, this should require $T < 30$ mK for appreciable polarization by thermal means, and such temperatures are not at all simple to achieve with H↓. The problem is largely due to a significant recombination pathway that is not completely suppressed by the high magnetic fields. That is, the ground spin state $| a \rangle$ is not the pure $| \downarrow\ddagger \rangle$ state (a simple arrow refers to the electron-spin, while a crossed arrow refers to the nuclear spin) but rather the admixture : $| \downarrow\ddagger \rangle - \varepsilon | \uparrow\ddagger \rangle$ where $\varepsilon = a/2\,\gamma_e H_0$ with $a/2\,\pi = 1.4$ GHz, the Fermi contact interaction of the H atom and γ_e, the gyromagnetic ratio of the electron. For fields of 10 T, $\varepsilon \simeq 2.5 \times 10^{-3}$. Thus there is still a small, but non-vanishing probability that the electron spin is up when in the spin ground state. This provides a recombination pathway provided at least one $| a \rangle$ state H atom is involved. While the heat generated by the recombination is a problem which limits the densities and temperatures achievable with H↓, there is another consequence that is of positive value. In time, H↓ in the $| a \rangle$ state « burns-off » leaving behind principally H↓ in the $| b \rangle$ state, which is a pure spin state : $| \downarrow\ddagger \rangle$ wherein both electron and nuclear spins are polarized down. The formation of « doubly spin-polarized » H↓ was originally inferred by the M.I.T. group from their kinetic data [11], and then directly confirmed at Amsterdam [12] by ESR and at Cornell [13] by NMR. The meta-stability of $| \downarrow\ddagger \rangle$ rests upon a nuclear T_1 « bottleneck » first proposed by Statt and Berlinsky [14] : namely that T_1, which is due to collisions between pairs of H↓ atoms, is much longer than the lifetime of H↓ due to the above recombination pathway (for the magnetic fields used). Thus, doubly-spin polarized : H↓‡ in the $| b \rangle$ state has a significant lifetime, permitting careful studies with it.

Let me summarize the properties of H↓‡ which will be important for the spin-wave phenomenon. In 10 T magnetic fields, the respective Boltzmann factors expressed as ratios of up to down spins are for 0.5 K (0.1 K) : electron (↓) : 10^{-11} (10^{-58}), proton 1.1(1.7), yielding a thermal nuclear spin polarization of order + 0.05(+ 0.25), while a recombination-induced polarization of nearly − 1.0 may be achieved. Our experiments are typically performed at densities of 10^{16}-10^{17} atoms/cm^3, for which the characteristic time scales in decreasing magnitude are nuclear $T_1 \sim$ hours, recombination times (for finite population of $| a \rangle$) $\sim$ 2-10 min, spin wave lifetimes $\sim$ 2 ms (as we shall see), inhomogeneous dephasing times (T_2^*) $\sim$ 80 μs, and mean collision times $\leqslant$ 1 μs. The important length scales are in increasing size : the s-wave scattering length between two H↓ atoms : $a_s \simeq 0.72$ Å (i.e. weakly repulsive), the thermal de Broglie wavelength in this temperature range is $\lambda_T \simeq$ 20-50 Å, the mean inter-particle spacing $d_1 \simeq$ 300-600 Å, the mean free path of H↓ : $l =$ 50-500 μm, the spin-wave wavelength $\lambda \simeq$ 0.1-1.0 cm and the sample size $L = 0.6 \times 1.0$ cm.

In order to perform this experiment, we employed a special cryogenic system for H atoms [15, 16], which also incorporates an NMR spectrometer [16]. The cryogenic system is sketched in figure 1. In this system gaseous H_2 at room temperature is dissociated into H atoms with a microwave discharge. It flows through teflon tubing at 80 K into the cryostat, but it is cooled only upon encounter with a radiation baffle that is coated with solid H_2 and is maintained at 10 K to minimize sticking and

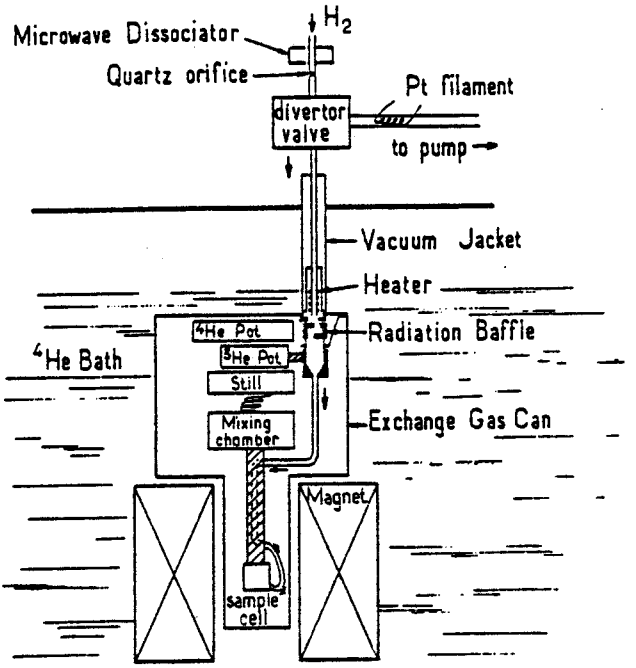

Fig. 1. — Schematic diagram of the cryostat and atomic hydrogen source. The flow of the atomic hydrogen is indicated by arrows. The thermal links from the ^{3}He refrigerator to the hydrogen flow tube and from the mixing chamber to the sample cell are indicated by the striped regions (from Ref. [16]).

[Schéma du cryostat et de la source d'hydrogène atomique. La direction de l'écoulement des atomes d'hydrogène est indiquée par des flèches. Les liaisons thermiques entre le réfrigérateur à ^{3}He et le tube où circule l'hydrogène, ainsi qu'entre la chambre à mélange et la cellule de mesure, sont indiquées par des zones hachurées (voir Ref. [16]).]

recombination. Just below this radiation baffle, the hydrogen atoms are cooled to 0.3 K by a continuous circulation ^{3}He refrigerator. All surfaces at or below 0.3 K that are exposed to H atoms are coated with a saturated film of superfluid ^{4}He, about 200 Å thick. The atomic H then travels into the region of high magnetic field, where the down electron spins are attracted but the up spins are repelled. Only the down electron spins reach the sample cell which is linked thermally to a dilution refrigerator. The H↓ enters the sample cell near the bottom. Temperature in the cell is monitored with bolometers, while pressure is measured by a strain gauge.

The 1 GHz NMR resonator, a split-ring or a « loop-gap » resonator (illustrated in Fig. 2), occupies most of the upper region of the cell. The loop-gap resonator consists of a metal tube with a slit along its length. The tube acts as an inductor which provides a rather uniform H_1 field, while the slit acts as a capacitor, wherein the E_1 field is contained. To prevent electrical breakdown in the presence of H↓ and ^{4}He, it was necessary to fill the capacitor gap with a high dielectric material. We used boron nitride, with which we also closed the ends of the tube. The resulting NMR sample region was then nearly a right circular cylinder with a length of about 1 cm and a diameter of 0.63 cm. The H↓ was allowed to enter the NMR sample region through a small hole in the resonator. The resonator is inductively coupled to a length of

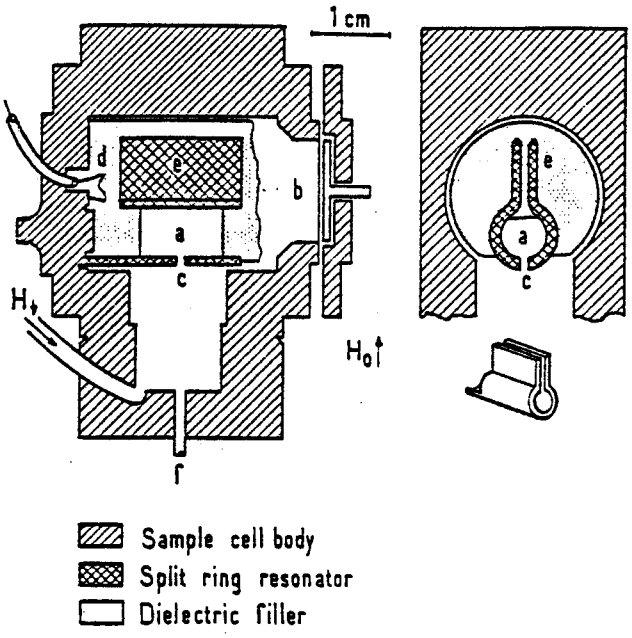

Fig. 2. — The sample cell. Left : a cross-section through the sample cell with the axis of the « loop-gap » or split-ring resonator in the plane of the paper. Upper right : a cross-section with the axis of the split ring perpendicular to the plane of the paper. Lower right : perspective view of the split ring, on a smaller scale. (a) is the NMR sample volume, (b) is the strain gauge, (c) is the entrance hole to the NMR sample volume, (d) is the coupling loop, (e) is the capacitor plates of the split ring, and (f) is the connection to the ^{4}He puddle (from Ref. [1]).

[La cellule de mesure. A gauche : une coupe de la cellule avec dans le plan du papier l'axe du résonateur en forme de cylindre coupé. En haut à droite : une coupe avec l'axe du cylindre coupé perpendiculaire au plan du papier. En bas à droite : vue en perspective du cylindre coupé à une plus petite échelle. (a) est le volume de la cellule soumis à la résonance RMN ; (b) est la jauge de contrainte ; (c) est le trou d'entrée du volume de la cellule où s'effectue la RMN ; (d) est la boucle de couplage ; (e) sont les plaques de condensateur du cylindre coupé ; et (f) est la connection vers la réserve d'^{4}He liquide (d'après Réf. [1]).]

coax leading to a pulse (and cw) NMR spectrometer that operates at 1 GHz and is located outside the cryostat. This spectrometer is described in Johnson's thesis [16].

Our usual method of operation was to apply a short pulse, corresponding to tipping the angle of the magnetization only slightly from the z-axis into the x-y plane. The free induction decay is then detected, digitized, and Fourier transformed. Signals from the resonator (about 0.3 cm^3 in volume) were strong enough that no signal-averaging over multiple pulses was required. This avoided any problems due to the changing nature of the H↓ sample during the course of the experiment. The minimum number of H↓ atoms inside the resonator that were required in order to see an NMR signal above the noise was about 3×10^{13} (for nuclear polarization of -1.0).

All our experiments were performed in the presence of field gradients G of the order of a few gauss/cm. The axial and radial components G_a and G_r could be varied by using the shim coils of the superconducting magnet providing the dc magnetic field (typically about 7.7 T in these experiments).

In our initial experiments we merely observed the free induction decay (FID) from a single short pulse. In fact, this provided initial evidence for the presence of the nuclear spin-waves. We show in figure 3 one such example. The main portion of the FID damps down in the characteristic time $T_2^* \simeq 80$ μs, but when the tail of the FID is observed for $t \gg T_2^*$ there is still a signal oscillating at a different (beat) frequency from the main portion, and it is found to have a lifetime ~ 2 ms.

When these FID's were Fourier Transformed (FT) the resulting frequency domain spectra provided even more convincing visual evidence of the presence of spin-wave modes. We show typical FT NMR spectra in figures 4 and 5, which are obtained with large negative spin-polarization (i.e. $P_z \leqslant -0.5$). These typical spectra consist of a broad resonance which contains a series of narrow resonance lines shifted to the right (high frequency) side of the spectrum. The overall width of the broad resonance could be varied from 3 kHz to 15 kHz by varying the field-gradient G, but it was only very weakly dependent on density, temperature, or nuclear-spin polarization. We observed that the broad resonance has the characteristics similar to an NMR spectrum from a sample of non-interacting spins experiencing a large magnetic-field gradient. For large negative P_z and/or low T there are typically many sharp lines, and one observes that the width of these lines increases monotonically as they are located closer to the center of the spectrum. The narrowest and most intense line is usually the highest frequency line.

In figure 4 we show spectra for which G is held constant while T is varied. The primary effect is a sharpening of the higher frequency lines with lowering T but not much change in the relative positions of these sharp lines nor of the overall width of the spectrum. In figure 5, we show spectra for constant T and density but G is varied. The larger gradient of the lower spectrum (Fig. 5b) is seen to produce more spin-wave modes that are more intense but on the whole broader and more separated. It also has a larger overall spectrum width than the upper spectrum.

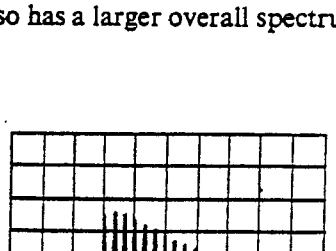

a) 20 μs/div

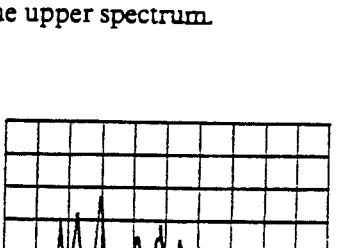

b) 200 μs/div

Fig. 3. — Free induction decays from H↓ in a field gradient. Curve (a) shows the decay of the main part of the signal with a $T_2^* \approx 80$ μs. The x-axis is 20 μs/division. Curve (b) shows under higher gain the long tail of the FID. The x-axis is 200 μs/division (unpublished results of Cornell group).

[Amortissement de la précession libre de H↓ dans un gradient de champ. La courbe (a) montre le déclin de la partie la plus grande du signal avec la constante de temps $T_2^* \simeq 80$ μs. L'échelle sur l'axe x est de 20 μs par division. La courbe (b) montre avec un gain plus grand la longue queue du signal ; sur l'axe x une division représente 200 μs (résultats non publiés du groupe de Cornell).]

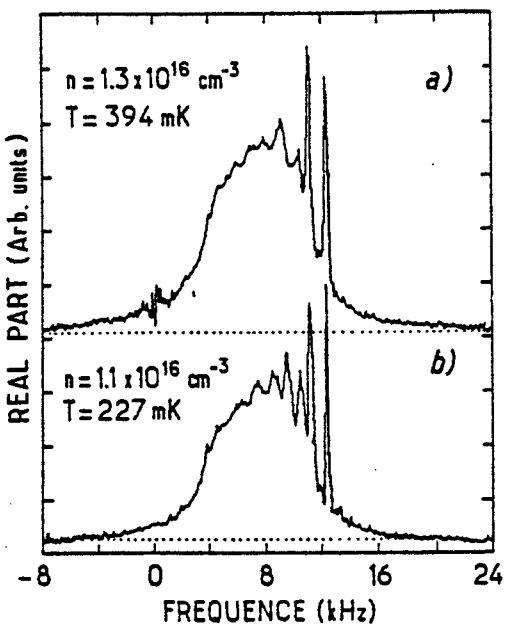

Fig. 4. — Typical small tipping-angle FT-NMR spectra for H↓. The field gradient was held constant (at $G_a \approx 0.6$ G/cm and $G_r \approx 3.5$ G/cm) while T was varied. (a) $T = 394$ mK, $n = 1.3 \times 10^{16}$ cm^{-3}; (b) $T = 227$ mK, $n = 1.1 \times 10^{16}$ cm^{-3}. There is large negative polarization [$-0.5 \geqslant P_z \geqslant -1.0$]. (The frequency axes are relative and they were aligned for the spectra to bring the highest frequency line into the same position) [from Refs. [1, 16]].

[Spectres RMN typiques de H↓ après transformation de Fourier pour de petits angles de basculement de l'aimantation. Le gradient de champ était maintenu constant (avec $G_a \approx$ 0,6 G/cm et $G_r \approx$ 3,5 G/cm) lorsque la température variait. (a) $T = 394$ mK, $n = 1{,}3 \times 10^{16}$ cm^{-3}; (b) $T = 227$ mK, $n = 1{,}1 \times 10^{16}$ cm^{-3}. Il y a une forte polarisation négative ($-0{,}5 \geqslant P_z \geqslant -1{,}0$). En ce qui concerne les fréquences en abscisses sur les deux courbes, les positions relatives des deux spectres ont été choisies de sorte que les raies de plus grande fréquence soient au même endroit pour les deux courbes (d'après les Refs. [1, 16]).]

One may ask whether there could be any anomalies arising from the Fourier transform of the time domain FID experiments. Even though the FID's and their FT's were performed with great care, we chose to confirm these results by performing some cw experiments. Care must be exercised to avoid saturating the cw spectrum, but our unsaturated cw-NMR spectra demonstrated very good agreement with the results of the FT-FID experiments [16].

We now wish to interpret these observations. In the absence of any spin-wave phenomena, the cw spectrum, or alternatively the FT of the FID, should be a single inhomogeneously broadened line, which provides an « NMR-Image » of H↓ distributed throughout the sample cell. Of course, there could be some averaging of the gradient due to diffusion of H↓ in the sample cell, but since $D/L^3 \ll \gamma G$ in our experiments, such averaging is marginal, and the cw line shape is just a single inhomogeneous line. The incipient effect of diffusion manifests itself in a spin-echo experiment wherein the large inhomogeneity is cancelled out. The original theory of Torrey [17] for diffusion of spins in a field gradient is then applicable, and it predicts an exponen-

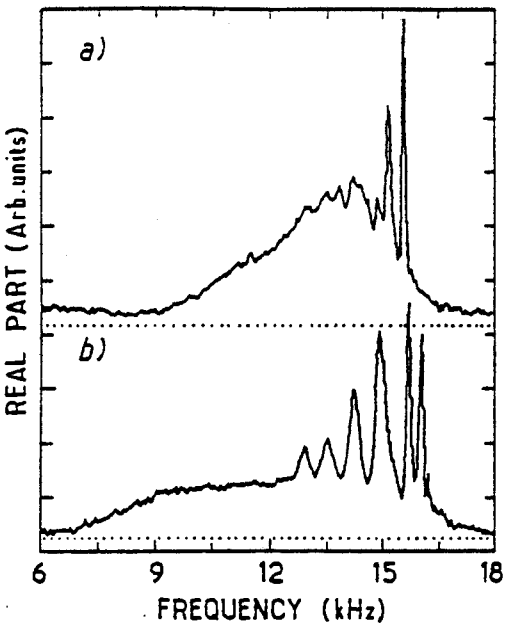

Fig. 5. — Variation of the FT-NMR spectra for H↓ with field gradient. The temperature is constant at $T = 245$ mK and the density nearly constant [3.6×10^{16} cm^{-3} for (a) and 3.2×10^{16} cm^{-3} for (b)]. Polarization is large and negative. Spectrum (b) is for a significantly larger gradient ($G_a \approx 1.6$ G/cm, $G_r \approx 1.0$ G/cm), than spectrum (a) ($G_a \approx 0.89$ G/cm, $G_r \approx 1.2$ G/cm). [Frequency axes are relative and have been shifted to compensate for different values of magnetic field] (from Refs. [1, 16]).

[Variation du spectre RMN de H↓ en transformée de Fourier en présence de gradient de champ. La température est constante à $T = 245$ mK et la densité presque constante ($3{,}6 \times 10^{16}$ cm^{-3} pour (a) et $3{,}2 \times 10^{16}$ cm^{-3} pour (b)). La polarisation est grande et négative. Le spectre (b) correspond à un gradient nettement plus grand ($G_a \approx 1{,}6$ G/cm ; $G_r \approx 1{,}0$ G/cm) que pour le spectre (a) ($G_a \approx 0{,}89$ G/cm ; $G_r \approx 1{,}2$ G/cm). (Les fréquences en abscisses sont relatives et les axes ont été déplacés de façon à compenser les variations dues aux valeurs différentes du champ magnétique (d'après les références [1, 16]).)]

tial decay according to $S(2\tau) = S(0)\, e^{-(2/3)D\gamma^2G^2\tau^3}$, where τ is the time between the two pulses (usually 90° and 180°) which form the echo at time 2τ. In the presence of boundaries, this result is, in general, modified [18], but again the slow-diffusion, large-gradient condition : $D/L^3 \ll \gamma G$ means that boundary effects would be negligible.

The presence of spin-waves drastically alters this story and leads to the narrow resonance lines that we observe (cf. Figs. 4 and 5). The existence of spin-waves in H↓ can be traced to the quantum-mechanical aspects of collisions between identical, hence indistinguishable, particles giving rise to an « identical spin-rotation » effect. Lhuillier and Laloë developed a detailed theory for the transport properties in spin-polarized boson (e.g. H↓) and fermion (e.g. ^{3}He) gases starting from a Boltzmann-type equation [5]. Lévy and Rückenstein [19] as well as Bashkin [6] have obtained similar predictions utilizing a many-body Hartree-Fock approach which emphasizes the relation to analogous effects in degenerate Fermi liquids. It is perhaps not sur-

prising, then, that the macroscopic effects of spin waves in H↓ follow a phenomenological law for the magnetization that is formally the same as that for degenerate Fermi liquids, namely a Leggett-Rice equation [20]. The spin-diffusion equation is :

$$\frac{\partial \mathbf{P}}{\partial t} - \gamma \mathbf{P} \times \mathbf{H}_0(\mathbf{r}) = D \sum_{i=1}^{3} \frac{\partial}{\partial x_i} \left[\frac{1}{1 + \mu^2 P^2} \left\{ \frac{\partial \mathbf{P}}{\partial x_i} - \varepsilon \mu \left(\mathbf{P} \times \frac{\partial \mathbf{P}}{\partial x_i} \right) + \right. \right.$$

$$\left. \left. + \mu^2 \left(\mathbf{P} \cdot \frac{\partial \mathbf{P}}{\partial x_i} \right) \mathbf{P} \right\} \right]. \quad (1)$$

Here $\mathbf{P}(\mathbf{r}, t)$ is the dimensionless vector spin polarization, $\mathbf{H}_0(\mathbf{r})$ is the dc magnetic field, which includes the field gradient, D is the diffusion coefficient for mass transport in H↓, μ is a parameter which describes the importance of the identical spin-rotation effect, while ε is + 1 for bosons and − 1 for fermions. It is μ which may be calculated by the Lhuillier-Laloë (LL) theory [5c]. In the limit of low T, when s-wave scattering dominates, one finds that $\mu = -\lambda_T/a_s$. Thus μ is also seen to be the measure of the relative importance of quantum-mechanical exchange effects in the collision of H↓ atoms, as mentioned above.

Equation (1) is seen to reduce to the Torrey equation in the semi-classical limit of $\mu \to 0$. When μ is non-negligible, there are non-linear corrections to the Torrey equation because of the « identical spin-rotation » effect due to the pairwise collisions of H↓ atoms with an *apparent* nuclear-spin-dependent collision cross-section. Of course, the true interaction potential is just that of the triplet potential curve [21], which is nuclear spin-*independent*. However, the effect of Bose statistics on the nuclear degrees of freedom leads to this apparent nuclear-spin dependence. There is, perhaps, a rough analogy with the familiar singlet and triplet potential curves for the interaction of two ordinary H atoms. As is well known, these potential curves arise from electron-spin independent Coulombic forces between the two atoms. It is only to satisfy the constraints of the Pauli Exclusion Principle for the identical electrons, that one can identify the bonding or singlet potential and the anti-bonding or triplet potential. The exchange interaction $2\,J(r_{12})\,\mathbf{S}_1 \cdot \mathbf{S}_2$ is the fictitious or « apparent » electron-spin-dependent potential term which may be formally introduced to account for the difference in the two potential curves. In an analogous manner, one may formally think of two spin-polarized H↓ atoms following the triplet electron-spin potential but showing an apparent nuclear spin exchange effect due to the requirements of Bose statistics. In fact, the identical spin rotation effect involves $\mathbf{I}_1$ and $\mathbf{I}_2$ both precessing about $\mathbf{I}_T \equiv \mathbf{I}_1 + \mathbf{I}_2$ which remains constant, consistent with such an exchange effect acting during their collision. This identical spin-rotation effect is described in more detail by Lhuillier and Leduc elsewhere in this volume [7a].

Another way to recover the Torrey result is to let $|P| \to 0$, i.e. to have H↓ with almost no nuclear-spin polarization. Then terms higher order in P than first order may be neglected. This arises from the LL-theory because successive collisions of a test H↓ with other H↓ atoms would involve precessions about randomly oriented axes tending to produce a zero resultant effect unless there were some preferential direction of alignment of the spins.

The non-linear form of equation (1) can lead to complex and interesting effects, but it is possible to perform experiments for which a linearized version of equation (1) is adequate. Suppose that initially $P_z \neq 0$, while $P_x = P_y = 0$ and P_z is uniform in space. Then a uniform, but small angle tipping pulse is applied to create a non-negligible $P_+ \equiv P_x + iP_y$. It will be true that $|P_+| \ll P_z| \simeq |P|$ and

$\nabla P_z \simeq 0$. In this limit equation (1) simplifies to the following two uncoupled equations :

$$\frac{\partial \tilde{P}_+}{\partial t} + i\gamma \tilde{P}_+ \, \delta H_0(\mathbf{r}) = \hat{D} \, \nabla^2 \tilde{P}_+ \tag{2}$$

$$\frac{\partial P_z}{\partial t} = D \, \nabla^2 P_z \, . \tag{3}$$

Equation (2) is for $\tilde{P}_+$ (i.e. P_+ in the frame rotating at the nuclear Larmor frequency), so it only depends on the field gradient term $\delta H_0(\mathbf{r})$, [i.e. $H_0(\mathbf{r}) = H_0 + \delta H_0(\mathbf{r})$]. While the z-polarization, P_z diffuses according to the normal diffusion coefficient D, the diffusion of the x-y polarization P_+ is described by an effective diffusion coefficient $\hat{D}$ which is complex :

$$\hat{D} = D \frac{(1 - i\varepsilon\mu P_z)}{1 + \mu^2 P^2} \, . \tag{4}$$

The real part of D represents a diffusion coefficient modified by identical particle exchange effects, while the imaginary part represents a cumulative phase shift due to the identical spin-rotation effect. [If we use the analogy to electron-spin exchange, $2 J(r_{12}) \, \mathbf{S}_1 \cdot \mathbf{S}_2$ a little further, this result is analogous to a damping plus a frequency shift generated by random spin-exchange collisions [22].]

Equation (3) (cf. also Eq. (1)) tells us that measurement of the z-magnetization, $M_z \propto nP_z$ (where n is the number density of H↓ atoms) from an initial non-uniform distribution of M_z (and $P_+ \simeq 0$) will allow D to be measured. Our experiment for measurement of D involves the application of a 180° pulse to the H↓ in the resonator that converts P_z to $-P_z$. This is then followed by a series of probing ε (i.e. small angle) pulses to monitor the return to the initial P_z (cf. Fig. 6). In these experiments, the return to the initial P_z occurs by diffusion of H↓ into and out of the resonator through the small hole connecting it to the rest of the sample chamber. This occurs much more rapidly than nuclear-spin T_1 processes. Our measurements lead to $nD = 1.9 \times 10^{18} \, \mathrm{cm^{-3} \, s^{-1}}$ for $n > 10^{16} \, \mathrm{cm^{-3}}$, a result that is rather independent of temperature over the range of 0.25-0.5 K studied (cf. Fig. 7). This is in good agreement with Lhuillier's predicted value [5c] of 1.5×10^{18} in this temperature region. (Below $10^{16} \, \mathrm{cm^{-3}}$, effects due to the mean-free-path becoming comparable to the dimensions of the hole, lead to a density-independent recovery time.)

What remains is to deal with equations (2) and (4). Let us first consider simple limiting cases. First suppose the sample is in free space with no field gradient. Then we obtain from the diffusion equation (2) travelling spin-waves that are damped, according to the simple dispersion-relation :

$$\omega_k = -D \frac{(\varepsilon\mu P_z + i)}{(\mu^2 P^2 + 1)} k^2 \, . \tag{5}$$

The boundaries will set up standing waves with discrete eigenvalues of k being allowed. In particular, we approximated the boundary conditions on the inner surface of the spherical resonator as :

$$\hat{\mathbf{n}} \cdot \nabla \tilde{P}_+(\mathbf{r}) = 0 \tag{6}$$

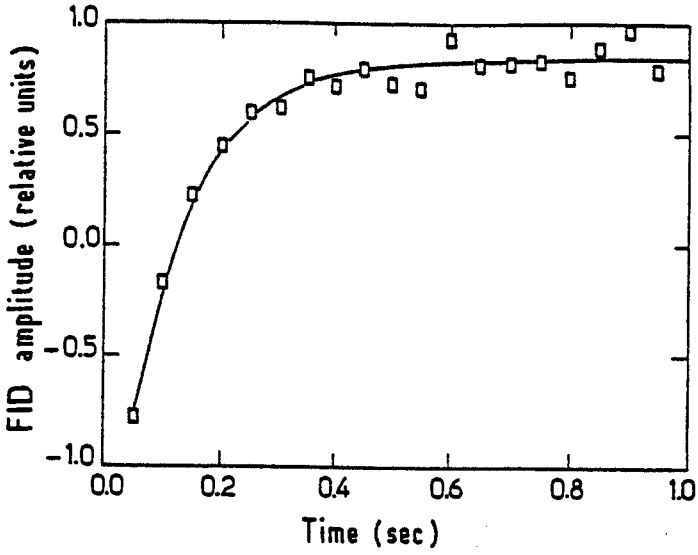

Fig. 6. — Recovery of z-magnetization of H↓ contained in the resonator after an initial π-pulse at $t = 0$ s. It is monitored by a series of small tipping pulses. The recovery is due to diffusion of H↓ into and out of the resonator (unpublished results of Cornell group).

[Relaxation de l'aimantation selon Oz de H↓ contenu dans le résonateur après une impulsion π initiale à $t = 0$ s. Elle est détectée par une série de petites impulsions de basculement. La relaxation est due à la diffusion de H↓ dans et hors du résonateur (résultats non publiés du groupe de Cornell).]

where $\hat{\mathbf{n}}$ is the unit normal to the surface. This is a « reflecting » boundary condition, which assumes that the H↓ are scattered off the surface with no change in their nuclear-spin properties, i.e. no significant nuclear-spin relaxation. Simple estimates of the effects of dephasing at the walls suggest this should not be unreasonable over the temperature range studied, but such dephasing effects are likely to be important below 0.2 K [16, 19].

Suppose we simply consider a one-dimensional standing wave subject to the boundary condition of equation (6). We let z' be the axis of the standing-wave. Then the solution of equations (2) and (6) are given as normal modes :

$$\psi_n = A_n \cos n\pi z'/L \qquad n = 0, 1, 2... \tag{7}$$

Thus the boundary conditions impose on the dispersion relation of equation (5) the discretization : $k_n = n\pi/L$. Such a standing-spin-wave mode is illustrated in figure 8.

However, when a field-gradient is present it acts as a large enough perturbation on the standing waves, that one must solve the associated eigenvalue problem. Here it is instructive to make use of the mathematical (but not physical !) analogy of the equation for P_- to a « Schrödinger Equation ». Let us first rewrite equation (2) as :

$$i\frac{\partial \tilde{P}_+}{\partial t} = i\hat{D}\,\nabla^2 \tilde{P}_+ + \gamma\delta H_0(\mathbf{r})\,\tilde{P}_+ . \tag{8}$$

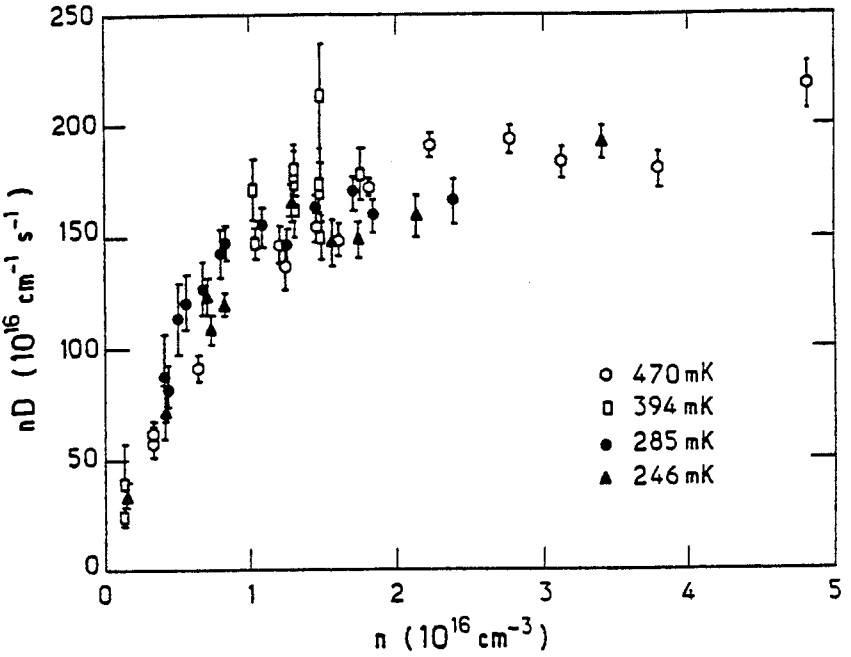

Fig. 7. — Diffusion coefficient as a function of density for several temperatures as noted in the figure. One finds $nD = 1.9 \times 10^{18}$ cm^{-1} s^{-1} for $n > 10^{16}$ cm^{-3} (unpublished results of Cornell group).

[Coefficient de diffusion en fonction de la densité pour plusieurs températures, comme indiqué sur la figure. On trouve $nD = 1{,}9 \times 10^{18}$ cm^{-1} s^{-1} pour $n > 10^{16}$ cm^{-3} (résultats non publiés du groupe de Cornell).]

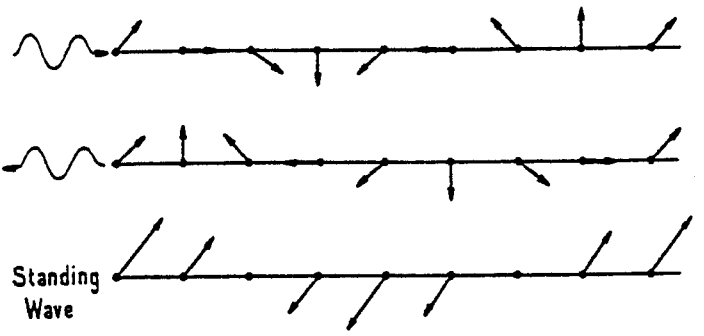

Fig. 8. — The transverse polarization. P_+ of two spin-waves travelling in opposite directions as a function of position, and the standing wave formed by their sum. There is no field gradient. The polarization rotates with time in the plane of the paper at each position. The sense of rotation is independent of the direction of wave propagation. Damping of spin-waves is ignored (from Ref. [16]).

[Polarisation transverse $\tilde{P}_+$ de deux ondes de spin se propageant dans des directions opposées en fonction de la position et l'onde stationnaire formée par leur somme. Il n'y a pas de gradient de champ. La polarisation tourne au cours du temps dans le plan du papier à chaque endroit. Le sens de rotation est indépendant de la direction de propagation de l'onde. L'amortissement des ondes de spin est ignoré (d'après la Réf. [16]).]

According to this formal analogy, $i\hat{D}\,\nabla^2$ plays the role of a « (complex) kinetic energy » operator, while the field gradient : $\gamma\delta H_0(\mathbf{r})$ that of a « potential energy » operator. We can now use familiar methods to solve for the spin-wave eigenmodes and their complex eigenfrequencies. In particular, we use eigenfunction expansion methods, with the basis functions taken as the standing-wave solutions to the diffusion equation in the absence of the field gradient and consistent with the reflecting boundary condition in our (approximate) geometry of a closed right circular cylinder.

These solutions are obtained numerically and are compared with experiments [16, 19]. Examples of our best fits between theory and experiment appear in figures 9 and 10. It is nevertheless possible to gain some insight into these damped spin-wave modes without the extensive computations required for quantitative accuracy. Let us consider the modes in the presence of a linear gradient that is axial, and we ignore any radial component in the cylindrical resonator. The normal modes in the presence of a large gradient may be obtained as follows.

From equations (4) and (8), we must solve the eigenvalue problem :

$$-D\left[\frac{-\varepsilon\mu P_z - i}{1+\mu^2 P^2}\right]\frac{\partial^2}{\partial z'^2}\psi + \gamma G z'\,\psi = E\psi \tag{9}$$

for complex eigenvalues E. We first consider the case where $\varepsilon\mu P_z$ is negative corresponding to a positive « Kinetic Energy » (but with damping) so that the analogy to a Schrödinger equation is most direct. For this case, we perform a change of variable

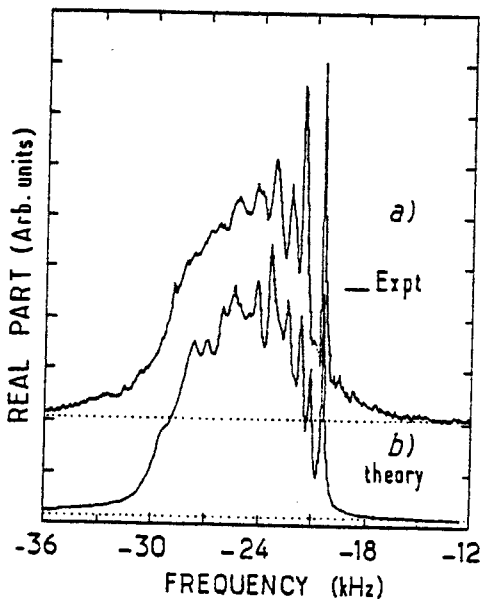

Fig. 9. — Comparison between experiment and theoretical prediction. It corresponds to $T = 227$ mK and $n = 1.1 \times 10^{16}$ cm^{-3}. The parameters used in the fit were : $\mu P = 5.0$, $D = 99$ cm^2/s, $G_r = 3.37$ G/cm, $G_a = 0.76$ G/cm (from Ref. [16]).

[Comparaison entre expérience et prédictions théoriques. Ceci correspond à $T = 227$ mK et $n = 1{,}1 \times 10^{16}$ cm^{-3}. Les paramètres ajustables utilisés sont : $\mu P = 5{,}0$; $D = 99$ cm^2/s ; $G_r = 3{,}37$ G/cm ; $G_a = 0{,}76$ G/cm (d'après la référence [16]).]

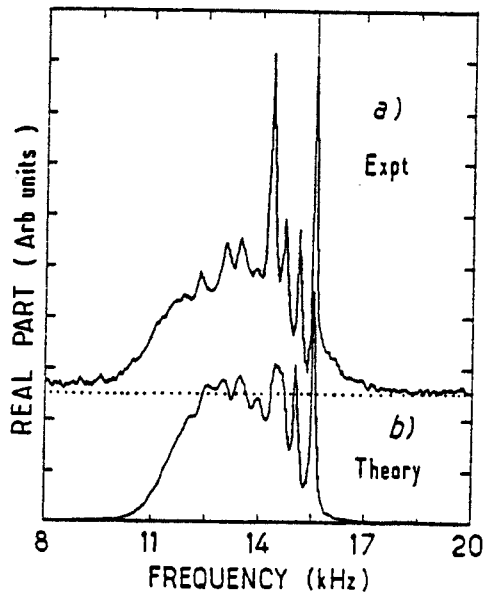

Fig. 10. — Comparison between experiment and theoretical prediction for the case of a smaller gradient than figure 9. It corresponds to $T = 247$ mK and $n = 3.7 \times 10^{16}$ cm^{-3}. The parameters used in the fit were : $\mu P = 6.0$, $D = 175$ cm^2/s, $G_r = 1.8$ G/cm, $G_a = 0.37$ G/cm (from Ref. [16]).

[Comparaison entre expérience et prédictions théoriques dans le cas d'un gradient plus petit que sur la figure 9. Ceci correspond à $T = 247$ mK et $n = 3,7 \times 10^{16}$ cm^{-3}. Les paramètres ajustables valent : $\mu P = 6,0$; $D = 175$ cm^2/s ; $G_r = 1,8$ G/cm ; $G_a = 0,37$ G/cm (d'après la référence [16]).]

to :

$$\xi = a_-^{-1}\left(z' - \frac{E}{\gamma G}\right) \tag{10a}$$

where a_- is a « characteristic length » given by :

$$a_\pm = \left[\frac{D}{\gamma G}\,\frac{\pm \varepsilon \mu P_z \pm i}{1 + \mu^2 P^2}\right]^{1/3} \tag{10b}$$

which yields the simpler differential equation :

$$\frac{\partial^2 \psi}{\partial \xi^2} - \xi \psi(\xi) = 0\,. \tag{11}$$

The solutions of equation (11) that are finite for all ξ are the set of Airy functions [23] :

$$\Phi(\xi) = A\,\frac{1}{\sqrt{\pi}} \int_0^\infty \cos\left(u\xi + \frac{1}{3}u^3\right) \mathrm{d}u\,. \tag{12}$$

We shall only consider the boundary condition at $z' = 0$, which from equation (6)

is just

$$\psi'(z' = 0) = \left.\frac{\partial \psi(z')}{\partial z'}\right|_{z'=0} = 0 .$$

We shall assume a large enough gradient G, that ψ has decayed virtually to zero when $z' = L$, so it is not necessary to invoke equation (6) at that boundary. This will be a reasonable approximation for the « lower energy » states when $|\mu P_z| > 1$. If we denote by α_n the roots of $\psi'(\xi)$, then we get from equation (10)

$$\psi'(z' = 0) = \psi'\left(\xi = \frac{-E}{\gamma G a_-}\right) = 0$$

and

$$\psi_n'(\alpha_n) = 0 \tag{13}$$

[where the Airy functions and their derivatives have zeroes only on the negative real axis [23]. In particular [23] : $\alpha_1 = -1.0188$, $\alpha_2 = -3.2482$, $\alpha_3 = -4.820$, $\alpha_4 = -6.1633$, $\alpha_5 = -7.3722$, while for large n one has $-\alpha_n \sim \left(\frac{3\pi}{2} n\right)^{2/3}$]. This yields :

$$E_{n_\mp} \equiv \omega_{n_\mp} = \mp \alpha_n a_\mp \gamma G = \mp \alpha_n \left[\gamma^2 G^2 D \frac{(\mp \varepsilon \mu P_z \mp i)}{1 + \mu^2 P^2}\right]^{1/3} \tag{14}$$

where the upper signs are to be used. The lower signs may be shown to apply to the case when $\varepsilon \mu P_z$ is positive. [One must first define a new $\xi = a_+^{-1}(z' - E/\gamma G)$ and let $z' = 0$ correspond to the opposite boundary, cf. Fig. 11.] The dispersion relation given by equation (14) shows a $G^{2/3}$ dependence on field-gradient and the weak 1/3 power dependence on D. For $|\varepsilon \mu P_z| \gg 1$ it also implies a weak $-1/3$ power dependence on $|\mu P|$ for the frequency shift but a $-4/3$ power dependence on $|\mu P|$ for the widths (cf. below). Qualitative trends of this sort may be discerned in our results. We see in figure 4 that by increasing $|\mu P|$ by lowering T, the spin-wave modes sharpen up but do not show any appreciable frequency shift. While in figure 5, we observe the significant effects on intensity, width, and frequency shift induced by changing the field gradient. However, this is a reduced sensitivity to D and μP compared to the plane-wave dispersion relation of equation (5), appropriate for zero field-gradient.

Equation (14) gives the complex « energies » of the discrete but damped spin-wave modes. Their eigenmodes are then expressed as Airy functions (cf. Eq. (12)) :

$$\psi_{n_\mp}(z') = A_{n_\mp} \Phi(\xi_{n_\mp}) = A_{n_\mp} \Phi\left(\alpha_n \pm \frac{z'}{a_\mp}\right) \tag{15}$$

for the two cases, with $A_{n_\mp}$ the normalization. It follows from equation (10b) that $a_+ = a_-^*$, so that $\psi_{n_+}(z') = \psi_{n_-}(-z')^*$ as required by the symmetry of equation (9). If we neglect damping (i.e. let $\mathrm{Im}\, a_- = 0$), then the Airy functions are oscillatory for $|z'| < |\alpha_n \mathrm{Re}\, a_-|$ and exponentially decaying for $|z'| > |\alpha_n \mathrm{Re}\, a_-|$, and we may regard $|z'| = |\alpha_n \mathrm{Re}\, a_-|$ as a « classical turning point ».

Equations (14) and (15) constitute the solutions to our simplified problem and typical confined spin waves are sketched in figure 11. We see that the lower energy modes are trapped by the linear potential well such that for $\varepsilon \mu P_z < 0$ they are on

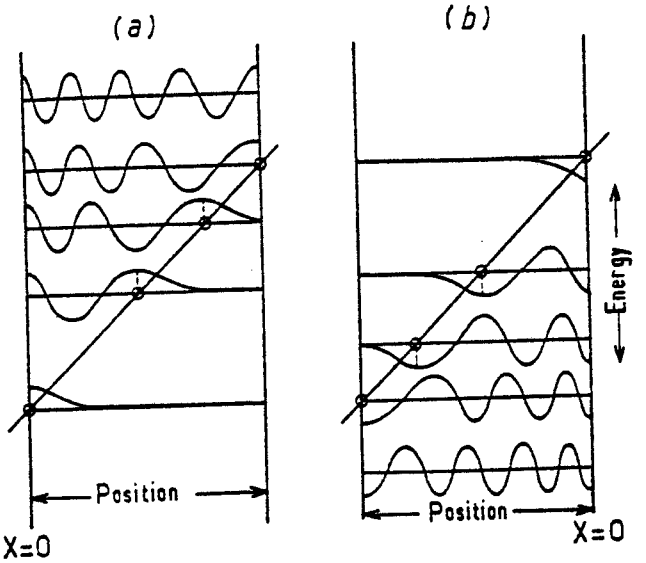

Fig. 11. — Sketch of spin wave modes between two reflecting walls in one dimension with a linear magnetic field gradient. The sloping line represents the « potential energy » due to this gradient. Case (a) is for $\varepsilon\mu P < 0$ while case (b) is for $\varepsilon\mu P > 0$. For case (a) the quantum numbers (hence « energies ») increase as one proceeds upward, while for case (b) they increase in an absolute sense as one proceeds downward. Damping is ignored. Circles show « classical turning points ». (The turning point for the lowest mode is actually slightly different from zero, cf. text.).

[Schéma des modes d'ondes de spin à une dimension entre deux parois réfléchissantes avec un gradient linéaire de champ magnétique. La courbe descendante représente « l'énergie potentielle » due à ce gradient. Dans le cas (a) on a $\varepsilon\mu P < 0$ tandis que dans le cas (b) on a $\varepsilon\mu P > 0$. Dans le cas (a) les nombres quantiques (c'est-à-dire les « énergies ») croissent lorsqu'on s'élève, tandis que dans le cas (b) elles croissent en valeur absolue lorsqu'on descend. L'amortissement est ignoré. Les cercles montrent les points de rebroussement du mouvement classique. Le point de rebroussement pour le mode le plus bas est en fait légèrement différent de zéro, voir texte.]

the left side of the cylinder, while for $\varepsilon\mu P_z > 0$ they are trapped on the right. Thus, if P_z changes in sign, the spin-wave modes must « move over » from one side of the cylinder and « reform » on the other side. In the limit of very large « kinetic energy », however, the effect of the field gradient may be neglected and instead we must consider the effects of the boundaries at $x = 0$ and L so that equations (5) and (7) become more appropriate approximations and these high « energy » modes are not localized.

It is convenient to define the quality factor Q of a spin-wave mode as the ratio of the magnitude of its frequency shift to its width (or inverse decay time). Then, for the high « energy » modes we have from equation (5) :

$$Q = |\varepsilon\mu P_z| . \tag{16a}$$

For the low « energy » case given by equation (14), we obtain in the limit $|\varepsilon\mu P_z| \gg 1$:

$$Q \approx 3\,|\varepsilon\mu P_z| . \tag{16b}$$

This emphasizes that for a large spin-rotation effect the frequency shift of the nth

mode is significantly greater than its width, and in fact leads to the sharp and distinct resonances from spin-waves of low n.

It should be noted that for a (nearly) uniform H_1 (or resonant) field, as utilized in our experiments, the limiting high « energy » modes for which equation (7) would be appropriate cannot be excited by the radiation. In fact, the lower the n of the solution to equation (14), the greater will that spin-wave mode be coupled to the resonant radiation. To understand this, we can define a « transition-moment » for the nth spin-wave mode :

$$d_n \equiv \frac{\gamma}{V}\int_V \psi_n(z)\, H_1(z)\, \mathrm{d}V = \frac{\gamma H_1}{L}\int_0^L \psi_n(z)\, \mathrm{d}z \tag{17}$$

where the equality follows for a homogeneous H_1. The « transition probability » for exciting the nth mode is just given by d_n^2. Equation (17) expresses the fact that the observable spectrum is the uniform integral over the whole sample. Clearly, when equation (7) is used, we obtain :

$$d_n = 0 \quad \text{for} \quad n > 0\,. \tag{18}$$

In the case of equations (14) and (15), we can expand the $\psi_n(x)$, given as Airy functions, in a Fourier series of the modes of equation (7), i.e. :

$$\psi_n(x) = \sum_{n'=0}^{\infty} a_{nn'} \cos\frac{n'\pi x}{L}\,. \tag{19}$$

Then we quickly see that :

$$d_n = a_{n,0}(\gamma H_1) \quad \text{for all} \quad n\,. \tag{20}$$

Physically, what is happening is that the trapped spin-waves are no longer oscillating uniformly in space, so that their space averages are no longer zero (cf. Fig. 11). As one goes to higher « energy » the portion of the spin-wave in the « classically accessible » region (which increases in size) is more like a simple sinusoid, so that portion does not contribute to d_n, but only the portion of the mode near the « classical turning point » does contribute. Thus the picture emerges, that as n increases, the spin-wave modes become relatively less coupled into the observable spectrum. For n large enough that the asymptotic form equation (7) is applicable, such modes no longer show up in the spectrum. Thus, in an approximate discussion, it is sufficient to consider only those modes for which the Airy functions are a reasonable approximation and to neglect the « higher energy » modes that are well-approximated by simple plane waves.

In our experiments, we are always in the limit that $|a_\pm|/L \ll 1$ corresponding to very effective trapping of the spin wave modes, so that equations (14) and (15) are quite representative, up through large values of n (i.e. for $|\alpha_n| \ll L/|\operatorname{Re} a_-|$ if damping is small). Thus, we see sharp and well-defined resonances to one side of the spectrum corresponding to the spin-wave modes of low n. The loss in resolution, for higher n may be analyzed from the asymptotic form for the α_n, namely :

$$-\alpha_n \sim \left(\frac{3\pi}{2}n\right)^{2/3}.$$

We do this by comparing the difference between the frequency shifts of two adjacent spin-waves *vs.* the sum of their widths, i.e. :

$$\left|\frac{\mathrm{Re}\,E_{n+1} - \mathrm{Re}\,E_n}{\mathrm{Im}\,E_{n+1} + \mathrm{Im}\,E_n}\right| = \left|\frac{\alpha_{n+1} - \alpha_n}{\alpha_{n+1} + \alpha_n}\right| Q \sim \frac{Q}{3n} \tag{21}$$

which for $n \gg Q/3$ amounts to a loss in resolution sufficient to achieve a broad envelope. In this regime the frequency shifts are unimportant, and this portion of the spectrum should be typical of an inhomogeneously broadened line in the limit of very slow diffusion, as indeed it is. Thus we see that in this eigenfunction-expansion analysis, the inhomogeneously-broadened resonance is itself made up of many spin-wave modes each of which makes only a small relative contribution. There is, in such respects, a close analogy between « spin-wave spectroscopy » and more conventional magnetic-resonance spectroscopy, for cases where the condition of motional narrowing is not fulfilled [25].

We turn now to the sign of the frequency shift, since this demonstrates the Boson property of the H atoms (i.e. $\varepsilon = +1$). Theoretical calculations by Lhuillier [5c] and confirmed by Lévy and Rückenstein [19] show that $\mu = -7.3$ for H↓ at 250 mK with μ going as $T^{-1/2}$ at low temperatures. Recall that the negative sign for μ is simply due to the fact that $a_s = 0.72$, i.e. the s-wave scattering is not repulsive from the triplet potential curve. Let us first consider the simple dispersion relation of equation (5). It tells us that if $\varepsilon\mu P_z > 0$ (e.g. corresponding to negative μ, positive ε for Bosons, and P_z negative), then the higher k modes will be shifted down in frequency relative to the low k modes. Similarly, the dispersion relation of equation (14) for $\varepsilon\mu P_z > 0$ (corresponding to the lower signs in equation (14)) again shows that the higher n modes are shifted down in frequency. On the other hand for $\varepsilon\mu P_z < 0$, the higher n modes in either case are shifted to higher frequency relative to the lower n modes. By comparison with all our experimental results, we find that when $P_z < 0$ we must have $\varepsilon\mu P_z > 0$, while for $P_z > 0$ it is the case that $\varepsilon\mu P_z < 0$. Thus for a negative μ, it must be that ε is positive !

We illustrate this in figures 12 and 13. In figure 12, a π-pulse is used to reverse the sign of P_z, which is initially negative. It leads to a reversal of the sense of the sharp lines (low « energy » modes) relative to the broad resonance. Similarly, in figure 13, P_z is initially positive due to thermal polarization while loading the resonator with H↓, but it soon changes to negative polarization due to preferential decay of the $|a\rangle$ spin states. Again we observe the appropriate shift in location of the sharp lines. We regard these experiments as good confirmations of the theoretical predictions as well as demonstrating the Boson character of H↓.

It may be amusing to reflect upon this spin-wave spectroscopy as a kind of « NMR-imaging ». Unlike the NMR imaging of classical objects by the use of field gradients, the spin-wave modes are themselves significantly altered by the field-gradients. Thus, we may state as the quantum uncertainty effect in NMR imaging of spin waves : the act of spatially resolving the spin-wave modes by applying a field gradient will in itself alter the spin wave modes so as to localize them in space (and allow them to be imaged). Alternatively, one may attempt to detect the spin-waves without altering them by a field gradient. This has been achieved for spin-waves from ^{3}He with a spatially-varying H_1 field that by symmetry couples directly to the lowest spin-wave mode [26], but such a technique has yet to be developed for H↓.

In the above we have focussed on the spin-wave modes obtained from the linearized Leggett-Rice equations with boundary effects. For large tipping angles the spectrum

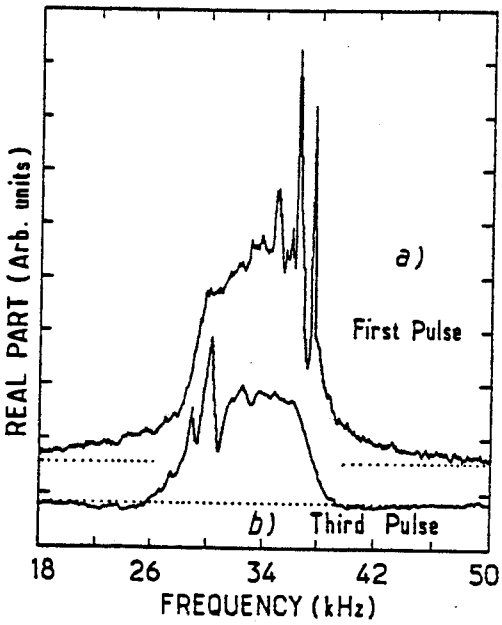

Fig. 12. — Reversal of the spin wave spectrum after rf-pulse inversion of the polarization. Spectrum (a) is obtained from the FID after the first pulse of an ε-θ-ε sequence, while spectrum (b) is obtained with the third pulse of the sequence. θ is approximately, but not exactly, equal to π, while $\varepsilon \approx \pi/4$. $T = 246$ mK, $n = 1.5 \times 10^{16}$ cm^{-3}, with field gradient the same as for figure 4 (from Ref. [1]).

[Renversement du spectre d'ondes de spin après retournement de la polarisation par une impulsion RF. Le spectre (a) est obtenu à partir du signal de précession libre après la première impulsion d'une séquence ε-θ-ε, tandis que le spectre (b) est obtenu après la troisième impulsion de cette même séquence. θ est approximativement, mais pas exactement, égal à π, tandis que $\varepsilon \approx \pi/4$. $T = 246$ mK; $n = 1{,}5 \times 10^{16}$ cm^{-3}; avec les mêmes gradients de champ que sur la figure 4 (d'après la référence [1]).]

becomes markedly different from the small tipping angle spectrum [16, 27]. In particular, the spectrum has a more complex structure, consisting of jagged peaks and deep troughs over the frequency range including the inhomogeneously broadened portion of the spectrum [16, 27]. Furthermore, while most of these lines are broader than the lines from the spin-wave modes in the small tipping-angle spectra, some new sharp lines are commonly seen in the large tipping angle spectra. Very recently Lévy has considered in detail analytic solutions for the one-dimensional Leggett-Rice equation for the non-linear spin-wave modes, and they suggest an impressive variety of non-linear phenomena which may be observed in such studies [28]. Other recent observations have included spin-echoes [29]. We observe normal echoes followed by several prominent peaks which resemble multiple echoes, and we have conjectured on their interpretation [29]. Lastly we note that, while electron-spin-wave modes have as yet not been seen in the laboratory, they should exist in principle and might be detectable under favorable circumstances [30].

In summary, our observations of nuclear spin waves in H↓ at Cornell dramatically demonstrate that it is possible to excite spin waves even in a rarefied gas, and they

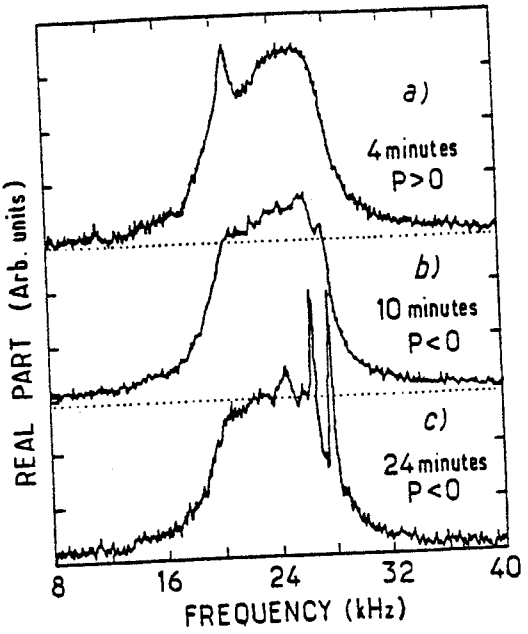

Fig. 13. — Evolution of the H↓ NMR spectrum over time due to recombination-induced polarization. Loading began at $t = 0$ and stopped at $t = 15$ min. Spectrum (a) was taken at $t = 4$ min. $T = 398$ mK, $n = 3.4 \times 10^{16}$ cm^{-3} and $P \sim +0.1$. Spectrum (b) was taken at $t = 10$ min, $T = 412$ mK, $n = 4.5 \times 10^{16}$ cm^{-3} and $P \sim -0.13$. Spectrum (c) was taken at $t = 24$ min (loading had stopped), $T = 393$ mK, $n = 2.4 \times 10^{16}$ cm^{-3} and $P \sim -0.6$. (Polarizations given are relative, their absolute magnitudes are only roughly estimated.) (from Refs. [16, 27]).

[Evolution dans le temps du spectre RMN de H↓ due à la polarisation induite par recombinaison. L'introduction de H↓ commence à $t = 0$ et finit à $t = 15$ min. Le spectre (a) est pris à $t = 4$ min, $T = 398$ mK, $n = 3{,}4 \times 10^{16}$ cm^{-3} et $P \approx +0{,}1$. Le spectre (b) est pris à $t = 10$ min, $T = 412$ mK, $n = 4{,}5 \times 10^{16}$ cm^{-3} et $P \approx -0{,}13$. Le spectre (c) est pris à $t = 24$ min (après arrêt de l'injection), $T = 393$ mK, $n = 2{,}4 \times 10^{16}$ cm^{-3} et $P \approx -0{,}6$. Les polarisations données ici sont relatives, leur valeur absolue est simplement estimée grossièrement (d'après les références [16 et 27]).]

have confirmed in considerable detail the theoretical predictions. In the future, as « spin-wave spectroscopy » becomes more precise, it should be possible to study interesting new non-linear wave phenomena and also to employ accurate measurements of spin-wave spectra to study detailed properties of the spin-polarized H↓. For example, it could provide a direct measure of the temperature of gaseous H↓ (*via* the dependence of μ on $T^{-1/2}$). This could permit the measurement of the Kapitza resistance between gaseous H↓ and the ^{4}He film, as well as to enable more accurate thermodynamic measurements on H↓. Such experiments might ultimately lead to observations of pre-transitional effects below n_c, the critical density, that are associated with the predicted BEC, and perhaps they could ultimately serve as a way of studying the actual BEC. The sensitivity to these properties of H↓ would, however, be enhanced by employing gradients in H_1 rather than in H_0, because the latter suppresses the dependence upon μ (and D) as we have seen.

Acknowledgments.

The author wishes to acknowledge the members of the Cornell $H\downarrow$ group both past and present whose collective work is reviewed herein : B. Yurke, B. R. Johnson, J. S. Denker, N. Bigelow, D. Thompson, K. Earle, A. Rückenstein, L. P. Lévy, B. Statt, T. Tommila and D. M. Lee. This work was supported by NSF grant # DMR-8305284.

References

[1] Johnson, B. R., Denker, J. S., Bigelow, N., Lévy, L. P., Freed, J. H. and Lee, D. M., *Phys. Rev. Lett.* **52** (1984) 1508.
[2] Johnson *et al.*, *Phys. Today* 37 (1984) 19.
[3] Lee, D. M. and Freed, J. H., *Phys. Today* 38, S-18 (Jan. 1985).
[4] Leduc, M., Trénec, G. and Laloë, F., *J. Physique Colloq.* **41** (1980) C7-75 ; Nacher, P. J., Tastevin, G., Leduc, M., Crampton, S. B., Laloë, F., *J. Physique Lett.* **45** (1984) L-441.
[5] a) Lhuillier, C. and Laloë, F., *J. Physique* 43 (1982) 197 ;
b) 43 (1982) 225 ;
also c) Lhuillier, C., *J. Physique* 44 (1983) 1.
[6] Bashkin, E. P., *JETP Lett.* 33 (1981) 8.
[7] a) Lhuillier, C. and Leduc, M., this volume.
b) Kleppner, D., this volume.
[8] Greytak, T. J. and Kleppner, D., Les Houches *New Trends in Atomic Physics*, edited by G. Grynberg and R. Stora, North-Holland, New York 1984, vol. II, p. 1127.
[9] Silvera, I. F., Proc. 16th Intl. Conf. Low Temp. Phys., *Physica*, **109-110B** (1982) 1499 ; Hardy, W. N., Morrow, M., Jochemson, R. and Berlinsky, A. J., *ibid.* (1982) 1964 ; Walraven, J. T. M. and Silvera, I. F. (to be published).
[10] Freed, J. H., *J. Chem. Phys.* 72 (1980) 1414.
[11] Cline, R. W., Greytak, T. J. and Kleppner, D., *Phys. Rev. Lett.* 47 (1981) 1195.
[12] Van Yperen, G. H., Silvera, I. F., Walraven, J. T. M., Berkout, J. and Brisson, J. G., *Phys. Rev. Lett.* 50 (1983) 53.
[13] Yurke, B., Denker, J. S., Johnson, B. R., Bigelow, N., Lévy, L. P., Lee, D. M. and Freed, J. H., *Phys. Rev. Lett.* 50 (1983) 1137.
[14] Statt, B. W. and Berlinsky, A. J., *Phys. Rev. Lett.* 45 (1980) 2105.
[15] Yurke, B., Ph. D. Thesis, Cornell University, 1983.
[16] Johnson, B., Ph. D. Thesis, Cornell University, 1984.
[17] Torrey, H. C., *Phys. Rev.* **104** (1956) 563.
[18] Robertson, B., *Phys. Rev.* **151** (1966) 273. Zientara, G. P. and Freed, J. H., *J. Chem. Phys.* 72 (1980) 1285.
[19] Lévy, L. P. and Rückenstein, A., *Phys. Rev. Lett.* 52 (1984) 1512.
[20] Leggett, A. J. and Rice, M. J., *Phys. Rev. Lett.* 20 (1968) 586 ; Legget, A. J., *J. Phys. C* 12 (1970) 447.
[21] Kolos, W. and Wolniewicz, L., *Chem. Phys. Lett.* 24 (1974) 457.
[22] Eastman, M. P., Kooser, R. G., Das, M. R. and Freed, J. H., *J. Chem. Phys.* 51 (1969) 2690.
[23] Abramowitz, M. and Stegun, I. A., *Handbook of Mathematical Functions*, Dover, New York (1965), p. 446.
[24] Note that our solution to equation (11) may be generalized by including both the Airy functions and their complementary functions [23] in order to allow for the rigorous boundary conditions at both $x = 0$ and L.

[25] SCHWARTZ, L. J., STILLMAN, A. E. and FREED, J. H., *J. Chem. Phys.* **77** (1982) 5410; MILLHAUSER, G. L. and FREED, J. H., *ibid.* **81** (1984) 37.
[26] TASTEVIN, G., NACHER, P. J., LEDUC, M. and LALOË, F., *J. Physique Lett.* **46** (1985) L-249.
[27] JOHNSON, B. R., BIGELOW, N., DENKER, J. S., LÉVY, L. P., FREED, J. H. and LEE, D. M., Proceedings LT-17, U. Eckern *et al.* Eds, Elsevier 1984, p. 451.
[28] LÉVY, L. P., private communication and preprint.
[29] DENKER, J. S., BIGELOW, N., THOMPSON, D., FREED, J. H. and LEE, D. M., Proceedings LT-17, U. Eckern *et al.* Eds, Elsevier 1984, p. 549.
[30] BOUCHAUD, J. P. and LHUILLIER, C., to be published.